ISSN 1063-7834, Physics of the Solid State, 2014, Vol. 56, No. 7, pp. 1391–1396. © Pleiades Publishing, Ltd., 2014.
Original Russian Text © S.V. Chuchupal, G.A. Komandin, E.S. Zhukova, A.S. Prokhorov, O.E. Porodinkov, I.E. Spektor, Yu.A. Shakir, A.I. Gribenyukov, 2014, published in Fizika Tverdogo Tela, 2014, Vol. 56, No. 7, pp. 1338–1344.

OPTICAL PROPERTIES

Mechanisms of Loss Formation in Nonlinear Optical Crystals $ZnGeP_2$ in the Terahertz Frequency Range

S. V. Chuchupal[a], G. A. Komandin[a], E. S. Zhukova[a, b], A. S. Prokhorov[a, b], O. E. Porodinkov[a, *], I. E. Spektor[a], Yu. A. Shakir[a], and A. I. Gribenyukov[c]

[a] *Prokhorov General Physics Institute, Russian Academy of Sciences, ul. Vavilova 38, Moscow, 119991 Russia*
** e-mail: oporodinkov@ran.gpi.ru*
[b] *Moscow Institute of Physics and Technology (State University), Institutskii per. 9, Dolgoprudnyi, Moscow oblast, 141700 Russia*
[c] *Institute of Monitoring of Climatic and Ecological Systems, Siberian Branch of the Russian Academy of Sciences, pr. Akademicheskii 10/3, Tomsk, 634055 Russia*

Received December 30, 2013

Abstract—Physical mechanisms of formation of radiation losses in the terahertz range in $ZnGeP_2$ crystals have been experimentally studied in the wave number range of 5–350 cm^{-1} at temperatures of 10–300 K. The dominant contribution of two-phonon difference processes to the loss formation in the given frequency range has been shown.

DOI: 10.1134/S1063783414070063

1. INTRODUCTION

The use of the terahertz (THz) frequency range (10^{11}–10^{13} Hz) necessitates the quantitative description of electrodynamic characteristics of advanced materials used in the development of active and passive elements for this range. Materials used for development of THz radiation sources are of special interest. One of the methods for generation of THz radiation is the generation at a difference frequency upon pumping of nonlinear optical crystals by two-frequency laser radiation [1–4]. Another method is the excitation of broadband THz radiation by femtosecond laser pulses [5–7].

A promising crystal in which both the methods for generation of THz radiation are realized is zinc germanium diphosphide $ZnGeP_2$. It has high nonlinear susceptibility and birefringence coefficients, sufficient for satisfying the conditions for the phase matching in wide spectral ranges [8]. The practical value of this crystal is also determined by its high optical breakdown threshold, good thermal conductivity, temperature, angular, and spectral synchronism widths, mechanical strength, and resistance to increased humidity and aggressive media [9].

The terahertz range is the region of the dispersion of various types of dipole absorption determining the losses of radiation generated in the nonlinear optical crystal itself. In [10], by submillimeter and infrared spectroscopy, absorption additional to phonon absorption was found in single crystal $ZnGeP_2$. It was shown that, at room temperature, this absorption has a diffuse character, i.e., is distributed in a wide frequency range without well-defined resonances. As a result, it was supposed that the determining role in the formation of dielectric losses in the THz range is played by free carriers.

Single crystal $ZnGeP_2$ is an indirect-band-gap semiconductor. In the literature, it is characterized by three band gaps determined by the structure of the valence band: A', B', and C'. The minimum band gap is 1.99 eV at room temperature [11, 12]. Due to the structural defects and vacancies in the band gap of these crystals, deep and shallow levels are formed. The presence of shallow levels, whose activation energy is about 0.6 eV, results in the enrichment of the spectrum in the mid-infrared region with additional absorption bands.

Free carriers in the conduction band, which are activated by two-photon absorption under the action of laser pulse [13], can also cause additional losses.

The aim of the present work is to reveal mechanisms forming the absorption in the submillimeter–THz spectral range in $ZnGeP_2$ and determine the parameters of this absorption.

2. EXPERIMENTAL TECHNIQUE, RESULTS, AND DISCUSSION

A $ZnGeP_2$ single crystal was grown by the technology presented in [14–16]. From the boule obtained, an oriented parallel-sided plate with a thickness of 0.405 mm was cut. The crystallographic axes **a** and **c** were located in the plane of the plate. The spectral measurements were performed in the frequency range

from 5 to 700 cm^{-1} at temperatures of 10–300 K for two polarizations: $\mathbf{E} \parallel \mathbf{c}$ and $\mathbf{E} \perp \mathbf{c}$. The transmission spectra were measured by a submillimeter backward wave oscillator (BWO) spectrometer "Epsilon" (5–32 cm^{-1}) [17] and a Bruker IFS-113v IR spectrometer (25–350 cm^{-1}). The IR spectrometer was also used for measuring the reflectance spectra in the range of 30–700 cm^{-1}. The polarizer was a metallic grid applied onto a 60-μm-thick polyethylene film. The parameters of IR-vibrations were determined in the Drude–Lorentz model with three fitting parameters: ν_i is the oscillator eigenfrequency; ε_i is the dielectric contribution to the static permittivity, γ_i is the damping of the ith oscillator, and ε_∞ is the high-frequency permittivity. In this case, the frequency dependence of the complex permittivity is expressed in the form of a sum of harmonic oscillators:

$$\varepsilon^*(\nu) = \varepsilon_\infty + \sum_{i=1}^{n} \frac{\Delta\varepsilon_i \nu_i^2}{\nu_i^2 - \nu^2 + i\nu\gamma_i}. \quad (1)$$

The calculated spectrum was fitted to the experimental data by minimizing the root-mean-square deviation of the model spectrum from the experimental one by varying the parameters of the dispersion model for calculating the reflectance spectrum:

$$R(\nu) = \left| \frac{\sqrt{\varepsilon^*(\nu)} - 1}{\sqrt{\varepsilon^*(\nu)} + 1} \right|^2. \quad (2)$$

When calculating the asymmetric strongly broadened bands, we used the model of interacting oscillators [18]:

$$\varepsilon_i^*(\nu) = \frac{s_i(\nu_2^2 - \nu^2 + i\nu\gamma_2) + s_2(\nu_1^2 - \nu^2 + i\nu\gamma_1) - 2\sqrt{s_1 s_2}(\alpha + i\nu\delta)}{(\nu_1^2 - \nu^2 + i\nu\gamma_1)(\nu_2^2 - \nu^2 + i\nu\gamma_2) - (\alpha + i\nu\delta)^2}, \quad (3)$$

$$s_i = \Delta\varepsilon_i \nu_i^2,$$

where α is the real part of the coupling constant, which determines the renormalization of the frequencies ν_i; δ is the imaginary part, which determines the deformation of the contours of absorption of interacting modes; and s_i is the oscillator strength ($i = 1, 2$).

Single crystal $ZnGeP_2$ belongs to the group of $A^{II}B^{IV}C_2^V$-type triple semiconductors. It has the structure of chalcopyrite (space group $D_{2d}^{12} = I42d$) with the lattice parameters $a = 5.465$ Å and $c = 10.708$ Å; the center of symmetry of the lattice is absent [19]. The elementary cell of $ZnGeP_2$ contains eight atoms, which corresponds to two formula units $Z = 2$. Factor group analysis admits the existence of 24 phonon branches. Long-wavelength normal vibrations are distributed over three types of symmetry: $A_1 + 2A_2 + 3B_1 + 4B_2 + 7E$. In the IR spectra, the modes $B_2(z)$ and $E(x, y)$ are active [20, 21].

Figure 1 shows the reflectance spectra measured at room temperature. We can distinguish with certainty two (Fig. 1a, $\mathbf{E} \parallel \mathbf{c}$) and four (Fig. 1b, $\mathbf{E} \perp \mathbf{c}$) IR-active

Table 1. Parameters of dispersion modeling of transmission–reflection spectra in THz and IR ranges of single crystal $ZnGeP_2$. $T = 300$ K, $\mathbf{E} \parallel \mathbf{c}$, and $\varepsilon_\infty = 10.2$ (IR-active phonons are emphasized by italic font)

Oscillator	Δε	ν, cm^{-1}	γ, cm^{-1}	δ, cm^{-1}
1.1	0.001	39	15	17
1.2	0.02	97	62	
2.1	*0.006*	*120*	*1.9*	*−9.5*
2.2	0.002	131	13	
3.1	0.006	191	29	2.6
3.2	0.008	209	38	
4.1	0.003	225	15	0.21
4.2	0.005	237	20	
5	0.002	254	11	
6	0.006	266	24	
7	0.01	288	15	
8.1	*1.3*	*342*	*3.5*	*−1.5*
8.2	*0.3*	*400*	*2.7*	
	$\Sigma\Delta\varepsilon_{phonon} = 1.6$			

Table 2. Parameters of dispersion modeling of transmission–reflection spectra in THz and IR ranges of single crystal $ZnGeP_2$. $T = 300$ K, $\mathbf{E} \perp \mathbf{c}$, and $\varepsilon_\infty = 9.7$ (IR-active phonons are emphasized by italic font)

Oscillator	Δε	ν, cm^{-1}	γ, cm^{-1}	δ, cm^{-1}
1.1	0.0009	39	15	−60
1.2	0.021	97	62	
2.1	0.007	136	17	−1.94824
2.2	*0.003*	*141*	*2*	
3	*0.004*	*142.5*	*2*	
4	*0.3*	*201*	*3.4*	
5	*0.5*	*327*	*5.9*	
6	*1.0*	*365*	*3*	
7	*0.3*	*384*	*1.3*	
	$\Sigma\Delta\varepsilon_{phonon} = 2.1$			

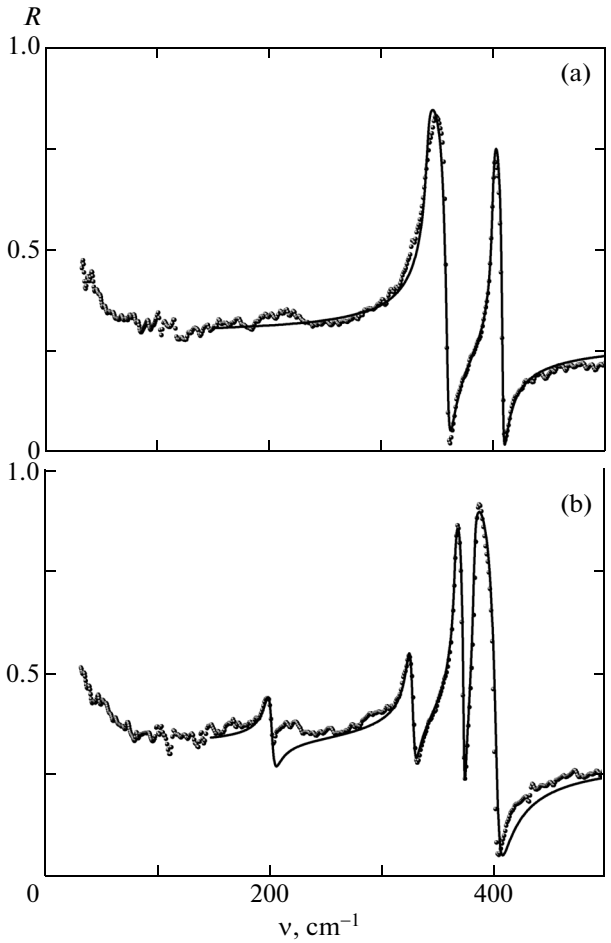

Fig. 1. Reflectance spectra (R) of single crystal $ZnGeP_2$ (points—experiment, lines—calculation) obtained for (a) $\mathbf{E} \parallel \mathbf{c}$ and (b) $\mathbf{E} \perp \mathbf{c}$.

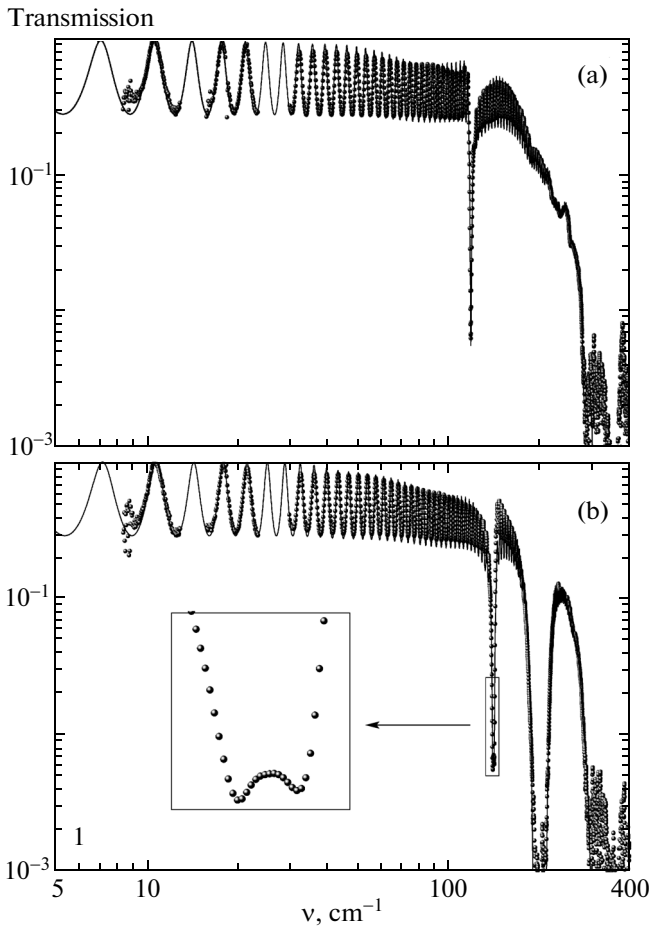

Fig. 2. Transmission spectra of single crystal $ZnGeP_2$ (points—experiment, lines—calculation) for polarizations (a) $\mathbf{E} \parallel \mathbf{c}$ and (b) $\mathbf{E} \perp \mathbf{c}$.

modes in the corresponding polarizations. We can see the deviation between the calculated and experimental spectra at the low-frequency edge of the range. It is explained by instrumental limitations of the IR Fourier spectrometer, which do not provide the sufficient accuracy of detecting the multi-beam interference in the transparency region of the sample. The interference was detected in the transmission spectra measured in the low-frequency part of the range.

The experimental transmission spectra in the corresponding polarizations are shown in Fig. 2. The resonance lines near 120 cm^{-1} for $\mathbf{E} \parallel \mathbf{c}$ (Fig. 2a) and 140 cm^{-1} for $\mathbf{E} \perp \mathbf{c}$ (Fig. 2b) correspond to IR-active phonons, which were not detected in the reflectance spectra due to the smallness of their dielectric contributions. It was found that the band in the vicinity of 140 cm^{-1} for the $\mathbf{E} \perp \mathbf{c}$ polarization consists of two closely placed resonance lines.

Tables 1 and 2 present the parameters of the dispersion modeling of the experimental reflectance and transmission spectra measured at room temperature in two polarizations. As is evident from the tables, the electron contribution ε_∞ into the dielectric permittivity exceeds approximately five-fold the total dielectric contribution $\Sigma\Delta\varepsilon_{phonon}$ of IR-active phonons. The anomalously high dielectric permittivity $\varepsilon_\infty \sim 10$ is also caused by the contribution of electron transitions from impurity levels in the band gap [19]. The small phonon contribution suggests a dominantly covalent character of chemical bonds in the $ZnGeP_2$ crystal with a relatively small fraction of ionic character.

From the parameters of dispersion modeling, the transmission spectra ($\mathbf{E} \parallel \mathbf{c}$) in the THz frequency range (Fig. 3) for two temperatures: 300 K (Fig. 3a) and 10 K (Fig. 3b) were calculated. We can see that the difference between the experimentally measured transmission spectrum and the spectrum calculated from the parameters of IR-active phonons is pronounced better at room temperature (Fig. 3a). Upon cooling the sample to 10 K, the deviation becomes minimal. At these temperatures, the spectra of dielectric losses $\varepsilon''(\nu)$ have been calculated (Fig. 4). The

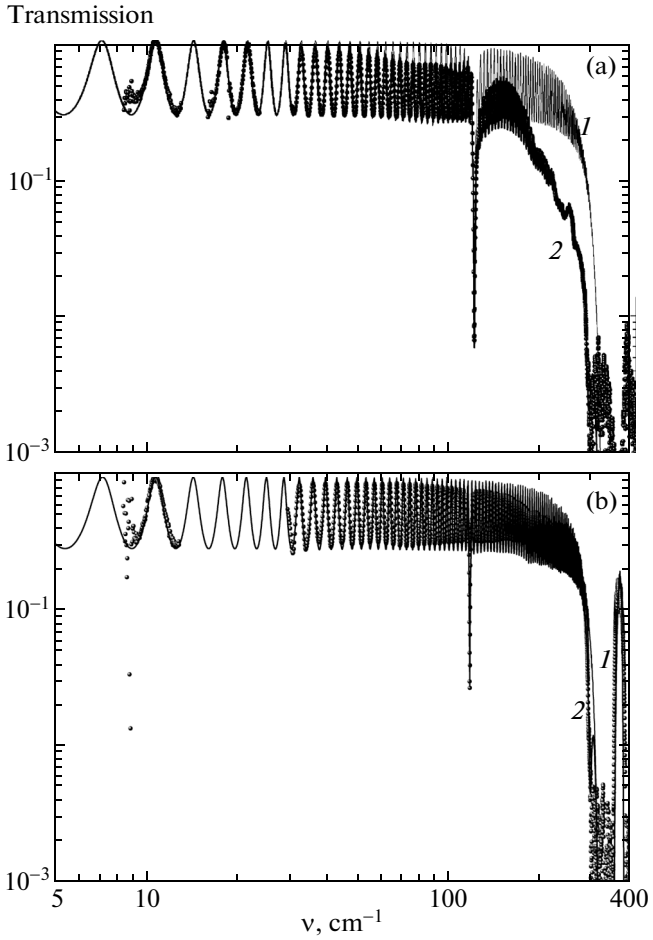

Fig. 3. Transmission spectra of single crystal $ZnGeP_2$ (**E** || **c**) at T = (a) 10 K and (b) 300 K. Points are the experimental data. Line *1* is transmission spectrum calculated from parameters of optical phonons, and line *2* is the transmission spectrum calculated from parameters of optical phonons with allowance for additional absorption.

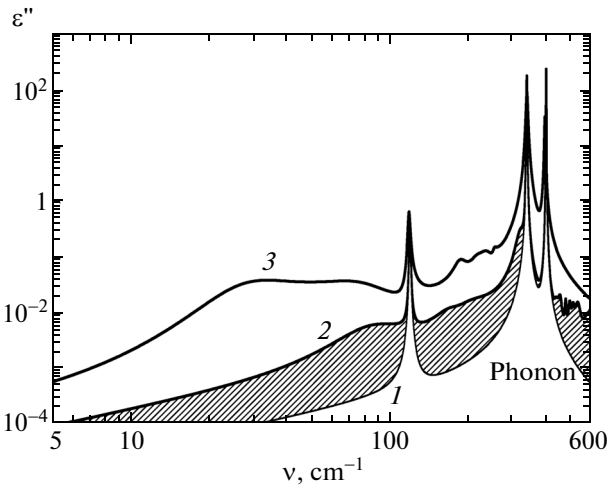

Fig. 4. Spectrum of the imaginary part of dielectric permittivity ε" of single crystal $ZnGeP_2$ for **E** || **c**. Line *1* is the spectrum ε" calculated from parameters of optical phonons at T = 10 K, line *2* is the spectrum ε" calculated from parameters of optical phonons with allowance for additional absorption at T = 10 K, and line *3* is the spectrum ε" calculated from parameters of optical phonons with allowance for additional absorption at T = 300 K.

comparison of the spectra shows that, at low temperatures, the residual contribution of the additional losses into the THz regions persists and the total loss in this case is reduced by an order of magnitude.

The increase in the transparency of the sample in the THz range upon cooling may be interpreted as a reduction in its conductivity [10]. The presence of a pronounced dispersion in the dielectric response spectrum in a limited frequency range does not agree with the classical Drude model of conduction

$$\sigma^*(\nu) = \frac{\sigma_0}{1 - i2\pi c\nu\tau}, \quad (4)$$

where σ_0 is the static conductivity and τ is the average time between successive collisions. Since the activation energy of the known interlevel transition correspond to the IR spectral region, the Drude model excludes noticeable dispersion of conductivity, caused by the presence of free carriers in semiconductors in the THz range [22].

The typical values of the static resistivity of $ZnGeP_2$ at room temperature are ~10^6–10^7 Ω cm. Substituting the value of the static conductivity into the Drude model and determining the transmission coefficient in the submillimeter-wave range have shown that the contribution of the conductivity on the level of 10^{-6} does not allow one to describe the experimentally observed absorption. Figure 5 shows the dynamic conductivity spectrum calculated from the parameters of dispersion modeling. The data presented imply that the role of conductivity in the formation of losses in the THz range is insignificant. The phonon contribution to the dynamic conductivity exceeds it by 2–3 orders of magnitude. Additional absorption mechanisms in the THz range increase this difference at least by an order.

Figure 6 shows the spectrum of dielectric loss ε"(ν) of single crystal $ZnGeP_2$ in the **E** || **c** polarization at room temperature. The dashed region under the total spectrum, denoted by *2*, shows the contribution additional to the phonon contribution, denoted by line *1*.

The additional losses are described in the model by a set of interacting oscillators (3). The calculation of the spectra by the Drude–Lorentz model (1) has shown that, upon cooling the sample, the oscillator eigenfrequencies in the THz range remain practically unchanged. In this case, the additional losses decrease. For IR-active phonons, we observe the ordinary narrowing of contours, caused by the reduction in the damping. The temperature evolution of the trans-

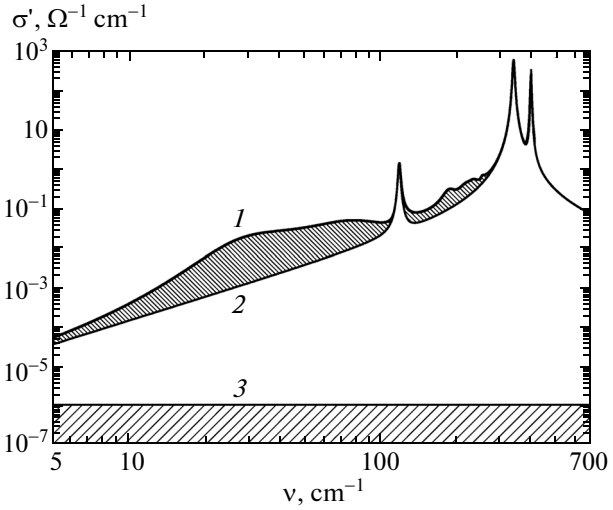

Fig. 5. Dynamic conductivity spectra of single crystal $ZnGeP_2$. Line *1* is the total conductivity spectrum obtained by simulation of the transmission and reflection spectra, line *2* is the phonon contribution to conductivity, and line *3* is the contribution to static conductivity.

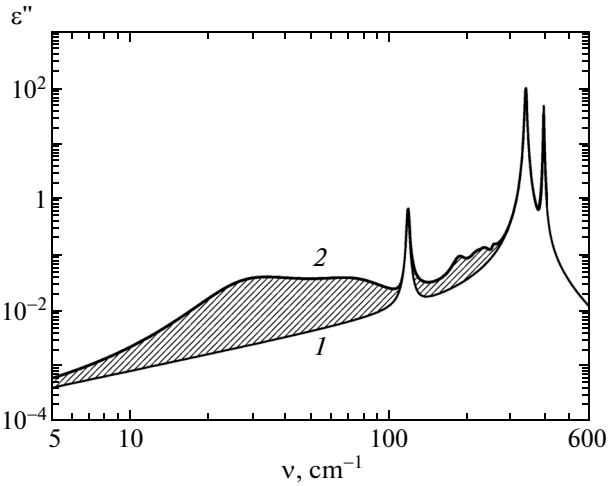

Fig. 6. Spectra of the imaginary part of dielectric permittivity of single crystal $ZnGeP_2$ ($\mathbf{E} \parallel \mathbf{c}$) at $T = 300$ K. Line *1* is the spectrum ε" calculated from parameters of optical phonons, and line *2* is the spectrum ε" calculated from parameters of optical phonons with allowance for additional absorption.

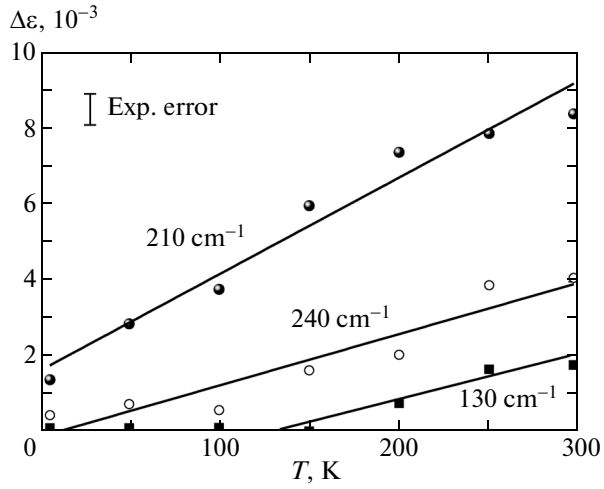

Fig. 7. Temperature dependences of the dielectric contributions $\Delta\varepsilon_i$ of single crystal $ZnGeP_2$ for different frequencies.

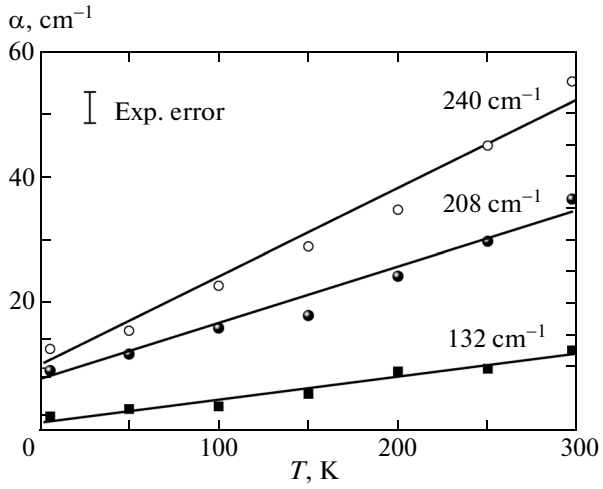

Fig. 8. Temperature dependences of the absorption coefficient α_i of single crystal $ZnGeP_2$ for different frequencies.

mission spectra in the THz range is described by the reduction in the dielectric contributions of model oscillators (Fig. 7).

As was noticed above, such a temperature dependence of the electrodynamic parameters in the THz range cannot be interpreted in the framework of the Drude model and excludes the phonon nature of the additional absorption because of the violation of the f-sum rule. The additional losses are interpreted in the framework of the model of multiphonon difference transitions in [23, 24], where the temperature dependence of absorption spectra, determined by the difference between the population of the optical and acoustical branches, is analyzed. In the approximation of a small temperature dependence of the population of the optical branch, we may assume that the intensity of transitions is determined by the occupation of the acoustic branch on the boundary of the Brillouin zone. The absorption in the region of difference two-phonon transitions is described by the linear temperature dependence [23] according to the Bose–Einstein law:

$$\overline{n}_i = \frac{1}{e^{(\varepsilon_i - \mu)/k_B T} - 1}, \quad (5)$$

where $\overline{n}_i$ is the number of particles in the ith state, ε_i is the energy of the ith state, μ is the chemical potential of the system, and k_B is the Boltzmann constant.

The obtained temperature dependence of the absorption coefficient at the frequencies corresponding to the difference multiphonon processes is shown in Fig. 8. The typical values of the model dielectric contributions describing these absorption processes do not exceed 10^{-2} [25].

Unlike simple two-atom ionic crystals considered in the cited works [23–25], single crystal $ZnGeP_2$ has more complex structure of the phonon branches in the Brillouin zone. The double folding of the Brillouin zone leads to an increase in the phonon state density and formation of residual THz absorption at low temperatures [26].

3. CONCLUSIONS

The experimental studies of single crystal $ZnGeP_2$ by THz and IR spectroscopy have revealed additional phonon absorption at the frequencies of 50–300 cm^{-1} with a pronounced temperature dependence. Asymmetric contours of this absorption have been described in the framework of the model of interacting oscillators. It has been established that the temperature dependence of model dielectric contributions and the frequency range of additional absorption dispersion suggest a dominant character of difference two-phonon processes, which, in addition to the one-phonon contribution and the increase in the phonon density of states due to the double folding of the Brillouin zone, form the dielectric losses in this crystal in the THz frequency range.

ACKNOWLEDGMENTS

This study was supported by the Department of Physical Sciences of the Russian Academy of Sciences within the framework of the Fundamental Research Program "Modern Problems of Radiophysics."

REFERENCES

1. R. L. Aggarwal and B. Lax, Top. Appl. Phys. **16**, 19 (1977).
2. V. V. Apollonov, A. I. Gribenyukov, V. V. Korotkova, A. G. Suzdal'tsev, and Yu. A. Shakir, Quantum Electron. **26**, 469 (1996).
3. K. Vijayraghavan, R. W. Adams, A. Vizbaras, M. Jang, C. Grasse, G. Boehm, M. C. Amann, and M. A. Belkin, Appl. Phys. Lett. **100**, 251104 (2012).
4. M. I. Bakunov, M. V. Tsarev, and E. A. Mashkovich, Opt. Express **20**, 28573 (2012).
5. R. Ulbricht, E. Hendry, J. Shan, T. F. Heinz, and M. Bonn, Rev. Mod. Phys. **83**, 543 (2011).
6. Y.-S. Lee, *Principles of Terahertz Science and Technology* (Springer-Verlag, New York, 2009).
7. J. D. Rowley, J. K. Pierce, A. T. Brant, L. E. Halliburton, N. C. Giles, P. G. Schunemann, and A. D. Bristow, Opt. Lett. **37**, 788 (2012).
8. V. G. Voevodin and V. A. Chaldyshev, Vest. Tomsk. Gos. Univ. **285**, 63 (2005).
9. G. Kh. Kitaeva, Laser Phys. Lett. **5**, 559 (2008).
10. V. V. Voitsekhovskii, A. A. Volkov, G. A. Komandin, and Yu. A. Shakir, Phys. Solid State **37** (7), 1198 (1995).
11. S. Limpijumnong, W. R. L. Lambrecht, and B. Segall, Phys. Rev. B: Condens. Matter **60**, 8087 (1999).
12. N. C. Giles, L. Bai, M. M. Chirila, N. Y. Garces, K. T. Stevens, P. G. Schunemann, S. D. Setzler, and T. M. Pollak, J. Appl. Phys. **93**, 8975 (2003).
13. S. M. Harrel, R. L. Milot, J. M. Schleicher, and C. A. Schmuttenmaer, J. Appl. Phys. **107**, 033526 (2010).
14. A. A. Vaipolin, V. Yu. Rud', Yu. V. Rud', and T. N. Ushakova, Semiconductors **33** (12), 1267 (1999).
15. G. A. Verozubova, A. I. Gribenyukov, and Yu. P. Mironov, Inorg. Mater. **43** (10), 1040 (2007).
16. G. A. Verozubova, M. M. Filippov, A. I. Gribenyukov, A. Yu. Trofimov, A. O. Okunev, and V. A. Stashchenko, Izv. Tomsk. Politekh. Univ. **321**, 121 (2012).
17. G. Kozlov and A. Volkov, Top. Appl. Phys. **74**, 51 (1998).
18. A. S. Barker, Jr. and J. J. Hopfield, Phys. Rev. A: At., Mol., Opt. Phys. **135**, 1732 (1964).
19. V. N. Brudnyi, V. G. Voevodin, and S. N. Grinyaev, Phys. Solid State **48** (11), 2069 (2006).
20. I. S. Gorban', V. A. Gorynya, V. I. Lugovoi, and I. I. Tychina, Sov. Phys. Solid State **17** (9), 1749 (1975).
21. Yu. F. Markov, V. S. Grigor'eva, B. S. Zadokhin, and T. V. Rybakova, Opt. Spektrosk. **36**, 163 (1974).
22. A. A. Volkov and A. S. Prokhorov, Radiophys. Quantum Electron. **46** (8–9), 657 (2003).
23. R. Stolen and K. Dransfeld, Phys. Rev. A: At., Mol., Opt. Phys. **139**, 1295 (1965).
24. M. Sparks, D. F. King, and D. L. Mills, Phys. Rev. B: Condens. Matter **26**, 6987 (1982).
25. G. A. Komandin, O. E. Porodinkov, I. E. Spector, and A. A. Volkov, Phys. Solid State **51** (10), 2045 (2009).
26. G. A. Komandin, E. S. Zhukova, V. I. Torgashev, A. V. Boris, A. A. Boris, E. A. Motovilova, A. S. Prokhorov, L. S. Kadyrov, B. P. Gorshunov, and M. Dressel, J. Appl. Phys. **114**, 024102 (2013).

Translated by E. Chernokozhin